# Analysis of Orbit Prediction Sensitivity to Thermal Emissions Acceleration Modeling for High Area-to-mass Ratio (HAMR) Objects

**Tom Kelecy**
*Boeing LTS, Colorado Springs, CO / Kihei, HI*
**Moriba Jah**
*Air Force Research Laboratory, Kihei, HI*

## ABSTRACT

High area-to-mass ratio (HAMR) inactive resident space objects (RSOs) in the geosynchronous orbit (GEO) regime pose a hazard to active GEO RSOs. The combination of solar radiation pressure (SRP), and solar and lunar gravitational perturbations causes perturbations in the orbits of these HAMR RSOs. The HAMR nature of these RSOs results in greater sensitivity to SRP forces resulting in the perturbation of mean motion, inclination and eccentricity. The subsequent drift with respect to the Earth, combined with time varying orientation with respect to the sun and transitions into and out of Earth's shadow, results in many of these RSOs being "lost" after initial acquisition as they transition through periods of days to weeks out of view of observing sites. This work examines the sensitivity of the prediction accuracies to inadequate modeling of the thermal emissions component of the SRP acceleration in the force models. The simplest models treat the thermal emission term either implicitly, or as a term that is a function of a fixed surface temperature and area. In reality, the temperature can vary with time for inert objects (e.g. orbital debris) transitioning in to and out of Earth shadow. Additionally, the orientation dynamics result in thermal acceleration components that vary relative to the inertial reference frame, and in general, have components orthogonal to the sun-object line. The prediction uncertainties associated with thermal modeling, orientation dynamics and materials uncertainties are examined in terms of the SRP acceleration perturbations for a range of representative HAMR object characteristics. Results indicate that significant prediction errors result from inadequate accounting for the thermal emissions component when compared to the standard SRP models used. These errors need to be addressed in the orbit determination and prediction to allow for more accurate re-acquisition and tracking.

## 1. BACKGROUND AND MOTIVATION

Schildknecht, et al [1] discovered a population of deep space objects thought to be debris having origins from sources in the geosynchronous orbit (GEO) belt. The international space community is actively involved in characterization of these objects as they pose a hazard to active RSOs operating in the vicinity of the GEO belt due to their large numbers and small size. The longitudinal variation resulting from the orbital perturbations, along with the dimness and variability of the visual magnitudes make them a challenge to track consistently and confidently. Their apparent small size makes them a dim optical object, and at GEO ranges, nearly impossible to track with radar. Nevertheless, repeated tracking of individual objects is crucial to making long-term observations with sensors that will provide better characterization of the material makeup of these objects, and to produce long-term orbital histories that might allow the debris to be associated with specific breakup events or objects of origin. The accurate orbit determination and prediction of these objects, and realistic characterization of the covariance, will help to mitigate the likelihood of collision with active maneuvering RSOs through collision probability assessment and collision avoidance.

Observations that have been conducted [1] indicate that HAMR objects have area-to-mass ratio (AMR) values ranging anywhere from 0.1 to 10's of $m^2$/kg, and thus explains observed variation of orbital parameters that distinguishes their long-term orbital histories. The SRP perturbation effects on orbital period, inclination and eccentricity can also produce significant variations over relatively short periods of time (days to weeks). The amplitudes and periods of the perturbations vary according to the magnitude of the AMR values [2].

Previous analyses have shown that HAMR objects have AMR values that vary with time [2,3], likely due to time varying SRP accelerations resulting from time varying solar illumination. It is hypothesized that the time varying solar illuminations are, at least in part, due to orientation changes with respect to the sun, and solar eclipsing periods. These in turn result in time varying reflective and emissive accelerations that are difficult, if not impossible to predict.

The purpose of this paper is to present a detailed SRP formulation which models the time varying orientation and surface thermal characteristics of HAMR objects in space, and to quantify the perturbation errors due to a

variety of modeling assumptions in the determination and prediction of the orbits of these objects. It will be shown that the errors due to the mismodeling of thermal emissions are large enough to result in significant errors in the orbit predictions and, in particular, can result in unbalanced accelerations in directions orthogonal to the object-sun line. The simulation results are compared to data derived from actual observations as a means to demonstrate the viability of the assumptions. The goal is that, by quantifying and bounding the errors and their distribution, the error information can be incorporated into the orbit determination process via representative process noise and/or more realistic covariance values, and ultimately improving the determination and prediction of these orbits to support characterization.

## 2. SOLAR RADIATION PRESSURE MODELING AND THERMAL EMISSIONS

The analysis in this paper examines perturbations resulting from modelling uncertainties associated with the SRP acceleration. It focuses on debris objects near the geosynchronous orbit regime having AMR values in the range of 0.1-20 $m^2$/kg. The gravitational perturbations are limited to the dominant zonal harmonic (J2) and luni-solar perturbations since the unknown HAMR dynamic effects are driven solely by non-conservative forces. The sensitivity to SRP perturbations given by the relatively HAMR values are of interest in assessing the orbital prediction sensitivity to mismodeling of SRP related parameters. Though subsequent work will address the impact to the orbit determination (OD) in detail, the results presented here will be used to outline their relevance to expected OD performance.

The SRP perturbation errors are analyzed in the radial, in-track and cross-track (RIC) position and velocity computed as the differences between an assumed reference trajectory and a perturbed trajectory integrated over the same span of time, geometry, etc. The SRP acceleration model used for this work incorporates both reflective and absorptive effects of the radiation incident on the RSO. The model accommodates any number of specified flat surfaces according to the equations

$$\vec{a}_{SRP} = -\frac{1}{c}\sum_{i=1}^{NS}\frac{A_i}{m}\{F_P \Phi \vec{R}_i\,(\hat{k}_i \cdot \hat{n}_i) + \vec{P}_i\} \tag{1}$$

where the specular and diffuse reflection terms for each surface are defined as

$$\vec{R}_i = (1-s_i)\,\hat{k}_i - \frac{2}{3}d_i\,\hat{n}_i + 2(\hat{k}_i \cdot \hat{n}_i)\,s_i\,\hat{n}_i \tag{2}$$

the emission term is defined as

$$\vec{P}_i = \frac{2}{3}a_i\,\sigma\,T_i^4\,\hat{n}_i \tag{3}$$

and the remaining parameters are defined as

$$\begin{aligned} c &= speed\ of\ light \\ s_i &= specular\ reflectivity\ of\ surface\ i \\ d_i &= diffuse\ reflectivity\ of\ surface\ i \\ a_i &= absorption\ of\ surface\ i \\ \sigma &= Stefan-Boltzmann\ const. \\ T_i &= temperature\ of\ surface\ i\ in\ \deg\ Kelvin \end{aligned}$$

The incident solar flux parameter, Φ, is adjusted according to the distance of the space object from the sun, but has a nominal (average) value of 1367 Watts/$m^2$ at distance of 1 Astronomical Unit (AU). Details of this computation can be found in [4,5,6]. The size parameter for each surface is defined as the area to mass ratio $A_i / m$ for surface area $A_i$ and mass $m$. The two unit vectors are defined as

$$\hat{k}_i = \textit{inertial unit direction of light incident on the surface}$$

$$\hat{n}_i = \textit{inertial unit surface normal of area } A_i$$

where it should be noted that

$$(\hat{k}_i \cdot \hat{n}_i) = \cos\textit{ine of the angle between incident light and unit surface normal}$$

is an attitude dependent parameter. The surface normal unit vectors are defined in a body reference frame, and must be transformed to the inertial reference frame. Finally, the parameter Fp (the shadow function), in the interval [0, 1], is critical in this analysis being that it is the function used to model passage into and out of Earth eclipse. The simplest geometric models are that of a cylinder or a conic/fractional, while the more complex pseudo-physical and physical models attempt to account for the effects of atmospheric refraction and absorption of the incident light rays.

The temperature variations are a function of the illumination angle, the time since shadow entry and its associated illumination angle, and the time since shadow exit as well as its associated illumination angle. Here, the illumination angle is defined as the angle between the incident sun vector and a vector normal (perpendicular) to a given surface. From the radiation pressure modelling work done to support precision orbit determination of the Topex/Poseidon mission [7] we model the temperature of a given surface while in sunlight as

$$T_i = k_1 + k_2 \cos(\theta_i / k_3)\{1 - \exp[-(t_1 + s_1)/k_4]\} \tag{4}$$

where

$$s_1 = -k_4 \ln[1 - \exp(-t_2 / k_5)(\cos\theta_{shd\_i} / \cos\theta_{sun\_i})] \tag{5}$$

And when the surface is in shadow, its temperature is modelled as

$$T_i = k_1 + k_2 \exp[-(t_2 + s_2)/k_5] \tag{6}$$

where

$$s_2 = -k_5 \ln(\cos\theta_{shd\_i} / k_3) \tag{7}$$

In the equations 4-7, $\theta_i$ is the angle between the surface normal and incident sun, $\theta_{sun\_i}$ is this angle when a surface enters sun illumination, and $\theta_{shd\_i}$ is the angle when a surface enters shadow. The surface material thermal parameters $k_1$ and $k_2$ are temperature lag model parameters, $k_3$ is a angle lag model parameter, and $k_4$ and $k_5$ are time lag model parameters.

An example of the error in the thermal emissions acceleration models is shown in Fig. 1 where the discrepancy between the fixed temperature and dynamic temperature models is plotted as a function of time. The three dimensional acceleration error is apparent in the plot. The resulting position perturbation over a 1 day span is shown in Fig. 2 where this representative GEO object has an AMR = 10 $m^2$/kg, and results in an in-track error growth approaching 30 km at the end of the one-day integration.

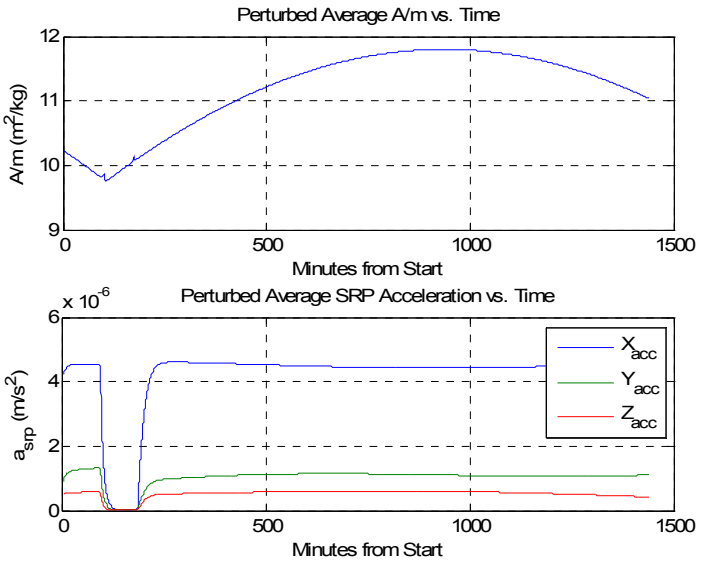


Fig. 1. AMR and Acceleration Error Profile for Constant vs. Variable Temperature Model

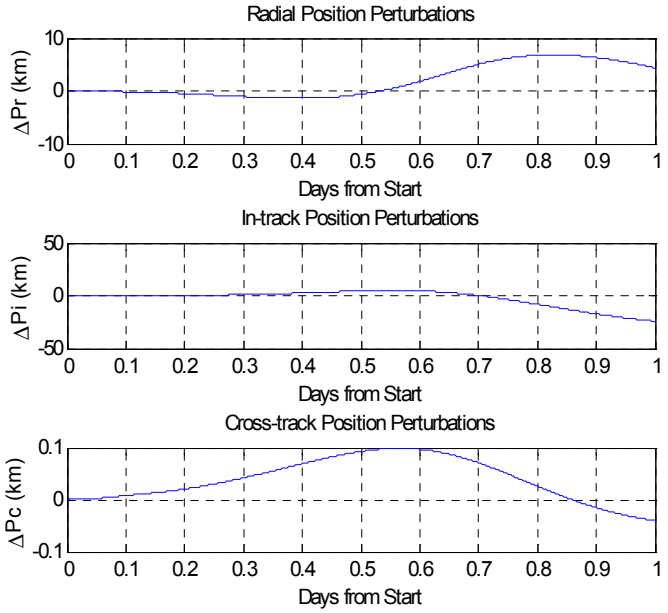


Fig. 2. AMR RIC Perturbation from Fixed vs. Dynamic Temperature Profile

## 3. THERMAL EMISSIONS ACCELERATION MODELING ERRORS

It is worth providing some actual evidence of the thermal emissions modeling errors by examining SRP solutions of a HAMR object tracked over a one-year span. In the KF estimation process for the object, a combined value of the AMR and the SRP coefficient

$$\gamma = \frac{c_R A_S}{m} \tag{8}$$

is actually estimated. If $c_R$ is assumed to be equal to 1, then the OD process is effectively estimating $A_S/m$. Note that mass is assumed fixed, and so $A_S/m$ variations are really just an indication of the object orientation changes resulting in variation of the cross sectional area exposed to the sun. All discussions of AMR throughout this work are taken to be synonymous with SRP.

The example HAMR for which a year span of angles-only data were available was processed using the Orbit Determination Tool Kit (ODTK) filter-smoother processing [8], where the extended Kalman filter (EKF) implementation allowed the AMR to be estimated dynamically at each measurement update. Two cases were processed. The first implemented dynamic stochastic estimation of the SRP to "optimize" the solution. The dynamic stochastic parameters were added in terms of "ecliptic north fraction" and "ecliptic planar fraction" components orthogonal to the sun-RSO line. The second case essentially had no dynamic stochastics added to the estimation process (i.e. the SRP was estimated as a constant bias parameter). In the case of the object examined, some level of dynamic stochastics was required in order to obtain acceptable solutions. The estimated AMR values over the period are shown in Fig. 3 in blue with respect to an nominal value of 0.946 $m^2/kg$, where the black lines in the figure indicate the ±2-σ state estimation error uncertainties. A seasonal component is apparent, in addition to the shorter period variations.

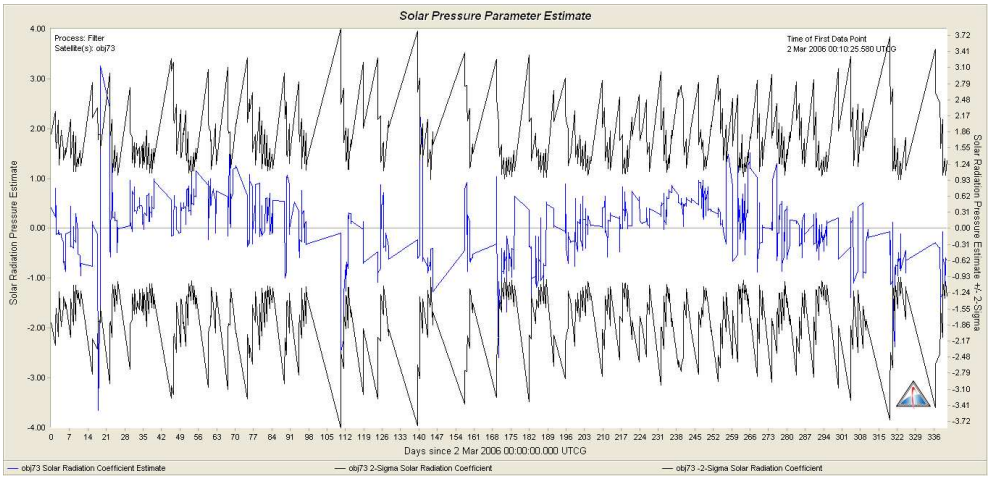


Fig. 3. Filtered SRP with Process Noise Added

In the filter solution where dynamic stochastics was applied, the "ecliptic north" and "ecliptic planar" factors of 4 were used for each component. The range of AMR variations in this case amounts to 0.5-4 $m^2/kg$ which can produce acceleration variations ranging from $2.2\times10^{-6}$ $m\text{-}s^2$ to $1.8\times10^{-5}$ $m\text{-}s^2$, and result in positional perturbations ranging from 10-100 km over a one day span as indicated in the corresponding lines of Fig. 4. It will be shown that these values are consistent with the simulation analysis results presented in the next section.

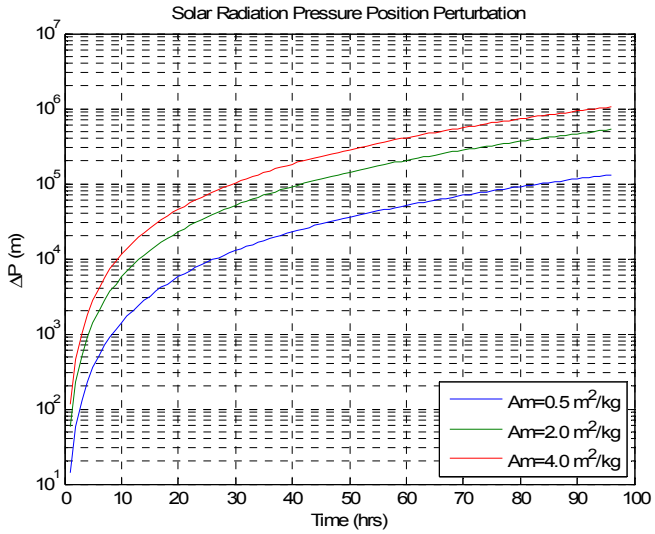


Fig. 4. SRP Perturbations from AMR Estimation Variations

Some justification for this argument is first in order by comparison with the case where no dynamic stochastics were added. The performance of the Kalman filter estimates, and the subsequent smoothing of the filter solutions, can be measured according to the consistency of the measurement corrections relative to the updated covariance. A measure of filter-smoother performance, known as the "McReynolds' consistency test", can be summarized by defining the following [9]:

$$X_k^f = \text{filtered state estimate at time } t_k$$

$$X_k^s = \text{smoother state estimate at time } t_k$$

$$P_k^f = \text{filtered covariance estimate at time } t_k$$

$$P_k^s = \text{smoother covariance estimate at time } t_k$$

then compute the estimated state and covariance differences between the filter and smoother:

$$X_{\Delta k} = X_k^f - X_k^s \tag{9}$$

$$P_{\Delta k} = P_k^f - P_k^s \tag{10}$$

Then for, the $i^{th}$ element of $X_{\Delta k}$ and the square root of the $i^{th}$ element of $P_{\Delta k}$ (sigma symbol) define the ratio

$$R_k^i = \frac{X_{\Delta k}^i}{\sigma_{\Delta k}^i} \tag{11}$$

If $|R^i_k| \leq 3$ for all $i$ and $k$, then the test is satisfied globally for each estimate. If $|R^i_k| > 3$ for all $i$ and $k$, then the filter-smoother test fails globally indicating the possibility of modeling inconsistencies. Thus, position, velocity and A/m estimation performance can be assessed in terms of the ratio of the estimates to the predicted/assumed modeling uncertainties.

The RIC position consistencies for the case with dynamic stochastics are shown in Fig.. 5., where the RIC position consistency values are less than the value of 3 for most of the measurement updates. In contrast to this, Fig. 6. presents the case where virtually no dynamic stochastics were added, and the result is that most of the consistency values exceeding the limit criteria.

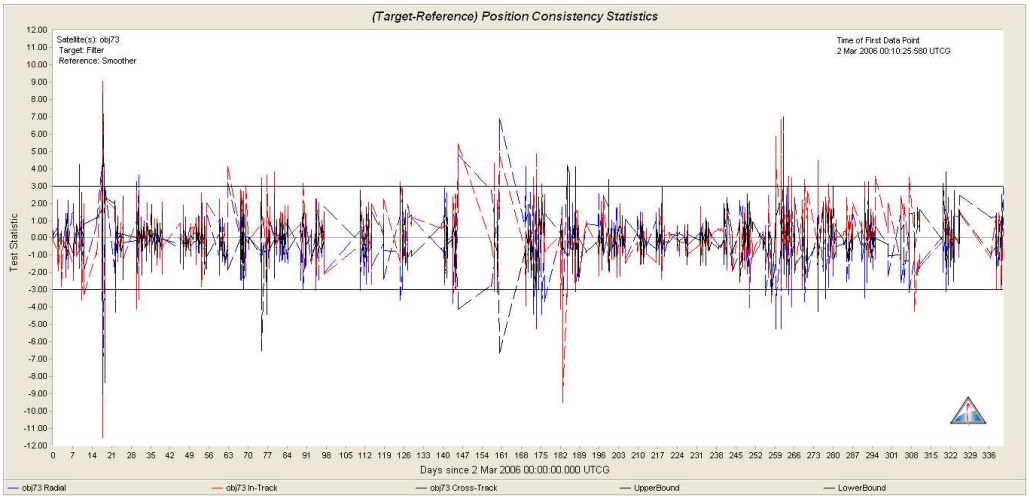

Fig. 5. RIC Position Consistency with Process Noise Added

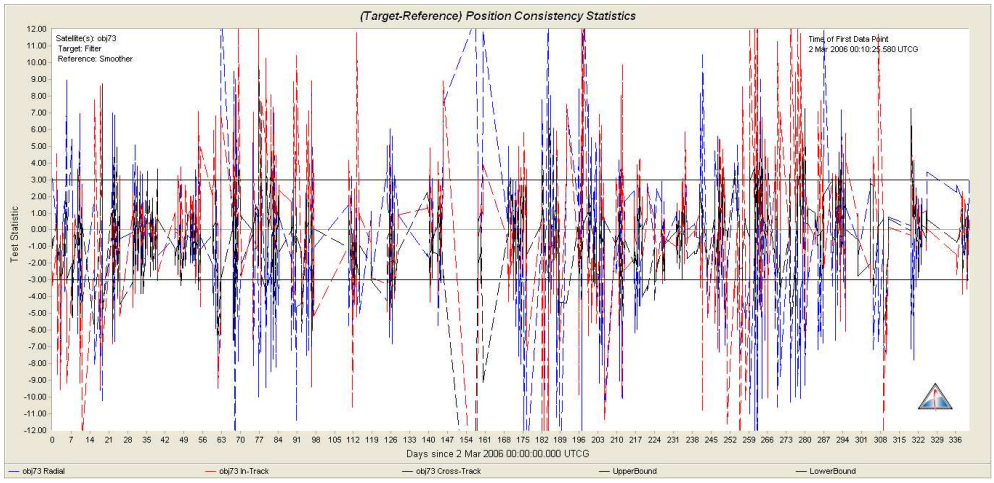


Fig. 6. RIC Position Consistency with No Process Noise Added

Similarly, the SRP consistencies where the dynamic stochastics were added are given in Fig. 7, and for the no dynamic stochastics case in Fig. 8. Again, the case where dynamic stochastics were added shows better filter-smoother consistency than the case without them. This supports the claim that there are unmodeled dynamic effects that must be accounted for.

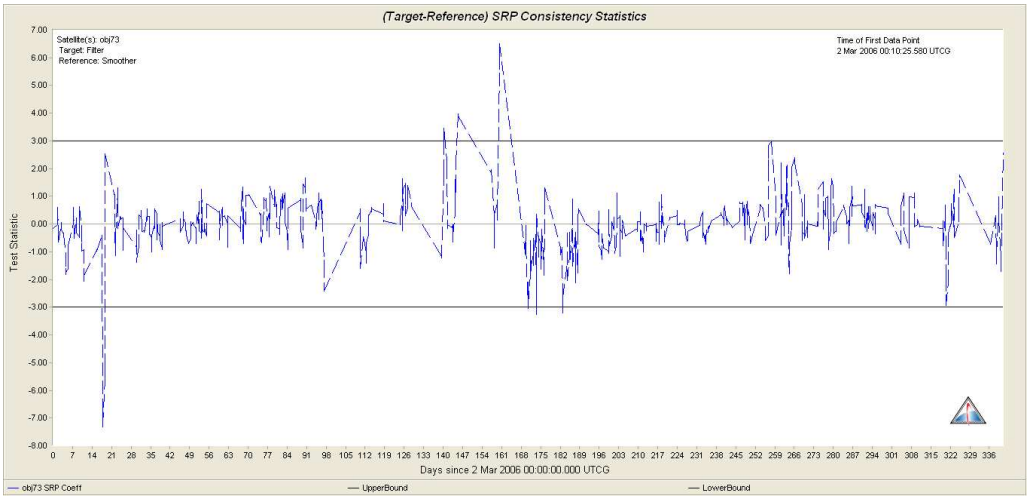


Fig. 7. SRP Consistency with Process Noise Added

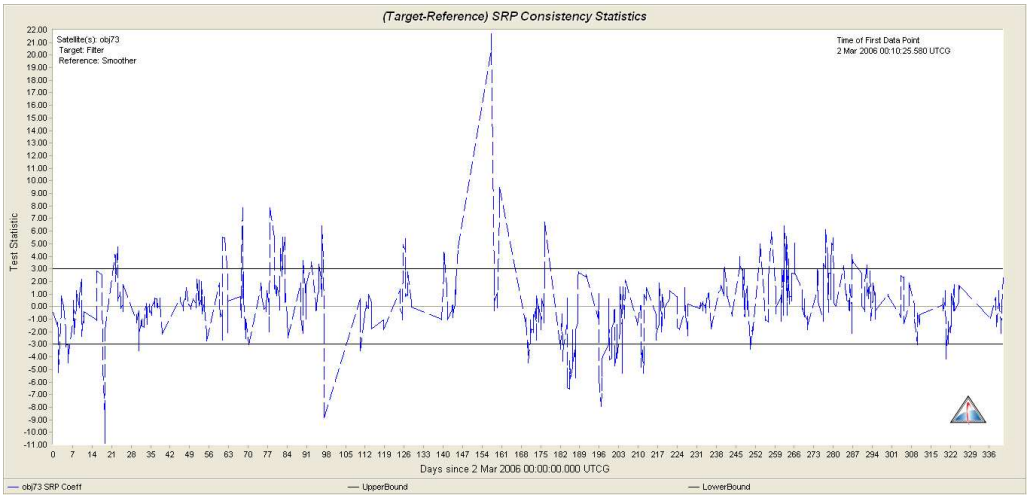


Fig. 8. SRP Consistency with No Process Noise Added

The ultimate impact of unmodeled dynamics is error in the OD solutions and subsequent predictions. The difference between the filtered and smoothed solutions is an indicator of prediction errors, as the filter predicts ahead based on the most recent measurement update while the smoother accommodates all of the data over the span analyzed. The filter-smoother differences for the case where dynamic stochastics were added are shown in Fig. 9, and can be compared to the larger differences for the case without them presented in Fig. 10. This illustrates the impact of unmodeled dynamics, and underscores the need to be able to quantify them, as this knowledge can be used in the judicious application of dynamic stochastics in the estimation process.

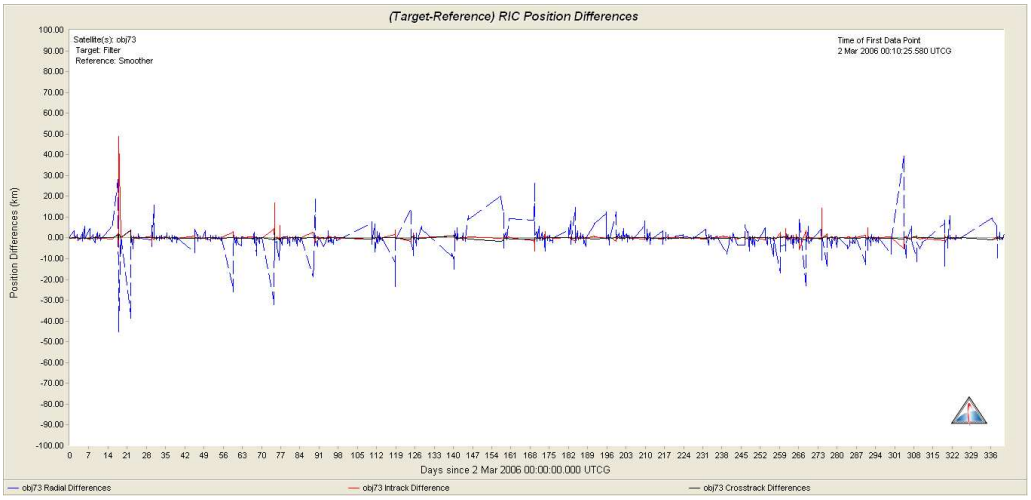


Fig. 9. Filter-Smoother RIC Differences with Process Noise Added

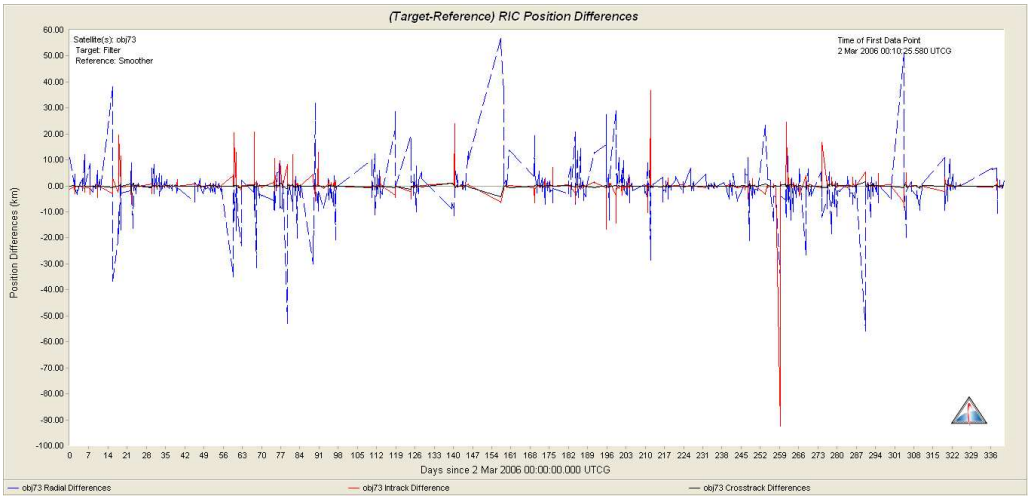


Fig. 10. Filter-Smoother RIC Differences with No Process Noise Added

## 4. MONTE CARLO ERROR ANALYSIS RESULTS

In order to analyze the complex interaction of the fixed surface temperature versus dynamic temperature assumption with the time varying illumination conditions, a Monte Carlo simulation was constructed in MATLAB to examine radial, in-track and cross-track (RIC) position and velocity errors for a range of orbit parameters and AMR values. The complex geometry of Earth eclipse due to diverse orbits was considered by examining a range of representative orbits, orientations, and spin rates.

It must be noted that the Monte Carlo analysis draws samples from assumed *a priori* distributions using MATLAB's pseudo-random number generator. Though the statistical distributions of the random parameters were assumed to be either uniform or normally distributed, increased observational data are needed to more accurately characterize the distributions.

The Monte Carlo simulation process is illustrated in Fig. 11, where each Monte Carlo trial creates a randomly sampled reference orbit and compares it to a perturbed orbit generated from randomly sampled initial conditions, namely orientation, reflection, thermal emission and AMR parameters.

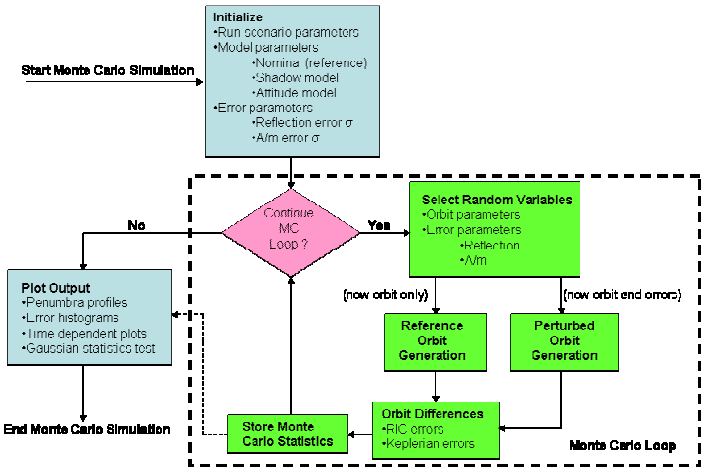

Fig 11. Monte Carlo Simulation Process

The 100 case Monte Carlo simulation was performed over a range of near GEO orbit parameters, and for a set of RSO model parameter errors. For the orbit, the semi-major axis ranged from 38,000-46,000 km, the eccentricity over 0.0-0.4, and the inclination from 0-10 degrees. Errors in the diffuse and specular reflectivity values, and the absorption, were 30% each, while the AMR values were uniformly distributed in the range of 0.1-20 $m^2/kg$. The epoch was chosen from Day-of-year 90-100 (one-day span around the spring equinox), with the radial, in-track and cross-track (RIC) position and velocity errors examined for a one-day propagation span. The mean, standard deviation and maximum deviation from truth(reference) for each of the RIC components (along with the total errors) were captured with the associated error distributions.

This first set of results are for the case where a constant surface temperature thermal emissions model was compared with a time varying surface temperature model using parameters typical of spacecraft materials [7]. The analysis was performed for the same randomly selected illumination conditions for both the reference and perturbed orbits. The resulting total position error distribution at the end of a one-day propagation period are shown in Fig.12 and indicate up to 100 km of error can be possible, with an average error in the range of 60-80 km over the range of AMR values.

The ±3-σ position errors by RIC component are shown in Fig. 13 over the one-day span, with the largest errors resulting in the in-track direction of over 100 km by the end of the propagation period, though errors result in all 3 of the components. The σ values are plotted relative to the means at each instant, and both mean and σ values are derived from the Monte Carlo results at the given time.

The second set of results are for the case where a constant attitude profile was compared with a time varying model using randomly selected rotation axes and rotation rates. This is a typical assumption, as there is usually no direct attitude information available on this class of RSO. The analysis was performed for the same randomly selected orbits and AMR values. The total position error distribution resulting at the end of a one-day propagation period is shown in Fig.14 and indicates up to 90 km of error can be possible, with averages of 40-60 km over the range of AMR values. Similarly, the ±3-σ position errors (relative to the mean error) by RIC component are shown in Fig. 15 over the one-day span, with the largest errors resulting in the in-track direction of over 100 km by the end of the propagation period, and errors again result in all 3 of the components.

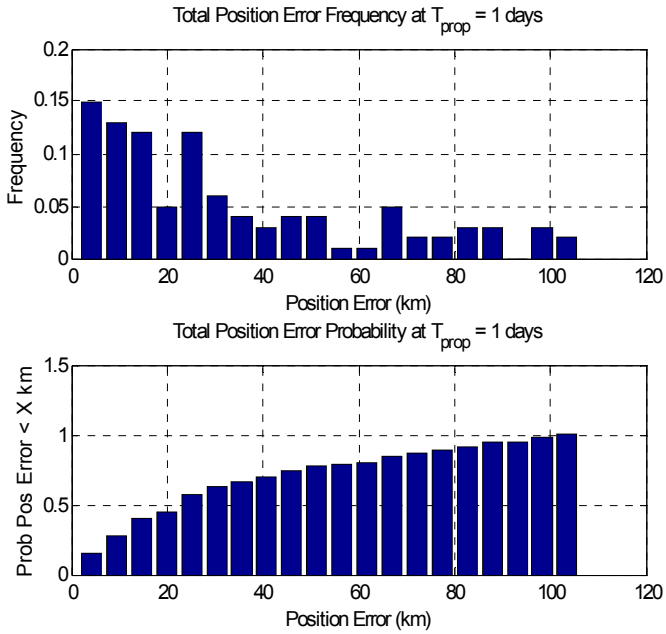


Fig 12. Position Error Distribution at one-day Propagation: vs. Dynamic Surface Temperature

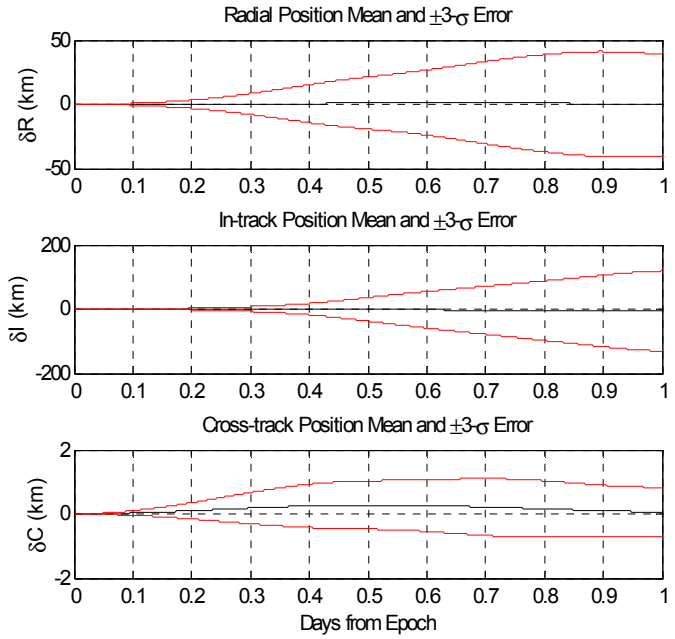


Fig. 13 RIC Position 3-sigma Uncertainties: Fixed vs. Dynamic Surface Temperature

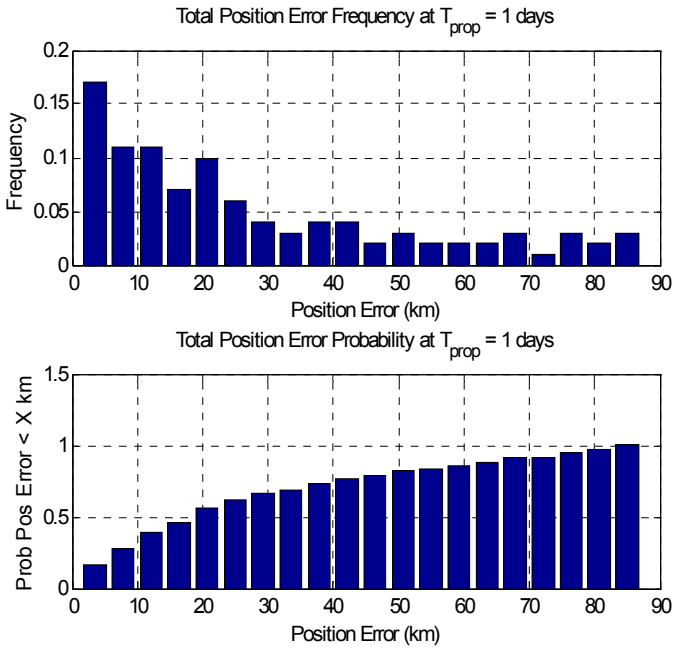


Fig 14. Position Error Distribution at one-day Propagation: Fixed vs. Rotating Attitude

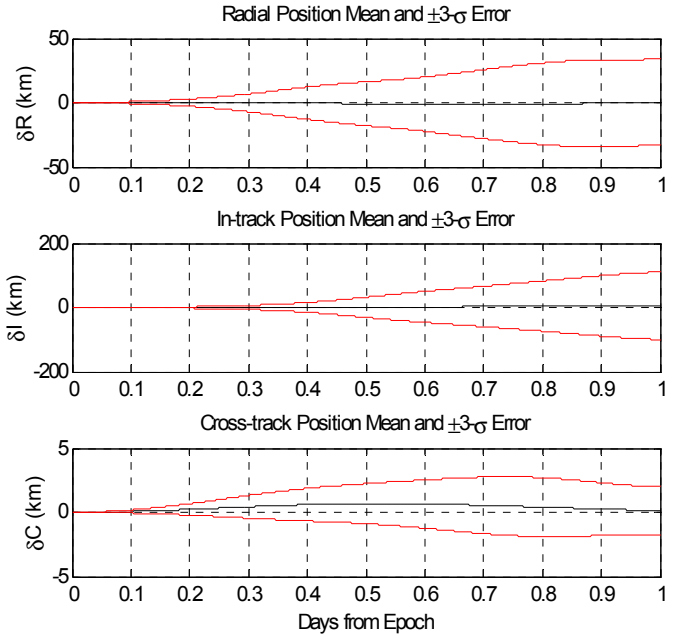


Fig. 15 RIC Position 3-sigma Uncertainties: Fixed vs. Rotating Attitude

## 5. CONCLUSIONS AND FUTURE WORK

The Monte Carlo simulation results yield the RIC errors of over 100 km resulting from a one-day propagation that assumes either constant surface temperature or fixed orientation with respect to time-varying surface temperature and/or attitude, where the errors result in non-Gaussian statistical distributions. The resulting errors are large enough to affect the loss of the object if reacquisition is attempted after several days or more. Future work will examine the impact of the assumption of non-normality of the trajectory errors over time, and motivates the investigation of making use of estimation strategies such as Adaptive Gaussian Mixture filters [10], which approximate the true PDF by way of fitting multiple Gaussian distributions to what is inferred from

the data. The "adaptive" aspect of this method is that in between observations, the relative weights assigned to each Gaussian component are propagated by constraining the weight estimates to minimize the predicted error in the Fokker-Planck-Kolmogorov equation. This equation is known to be the theory which describes the true evolution of any PDF.

It is evident that adding the dynamic stochastics improves the estimation accuracy, as they account for the dynamic SRP mismodeling. The question arises as to whether we recover information about the orientation to fold back in to the dynamic models so as to improve our predictions. For sparse data, only long-term variations might be recovered if periodic observations can be made. Assessment of the ability to recover meaningful information about an RSO given data sparseness, force models that can incorporate this level of detail, and the estimation algorithms that use them, are the focus of present research and development.

## 6. ACKNOWLEDGEMENTS

We would like to acknowledge the Air Force Research Laboratory for funding support of this work, Tim Payne and Robin Thurston of the U.S. Air Force Space Command for providing the data for the processing example, the good people at AFRL and Boeing who provide review and public release support, and last but not the least, we both acknowledge our families for their unwavering support of us in the important work that we do to help protect our great nation.

## 7. REFERENCES

1. Schildknecht, et al., "Properties of the High Area-to-mass Ratio Space Debris Population in GEO," AMOS Tech. Conf., Wailea, Hawaii, Sept, 2005.
2. Kelecy, Tom, Tim Payne, Robin Thurston and Gene Stansbery, "Solar Radiation Pressure Estimation and Analysis of a GEO Class of High Area-to-mass Ratio Debris Objects", AAS 07-391, AAS Astrodynamics Specialist Conference, Mackinac Island, MI, August 2007.
3. Kelecy, T., E. Baker, P. Seitzer, T. Payne and R. Thurston, "Prediction and Tracking Analysis of a Class of High Area-to-mass Ratio Debris Objects in Geosynchronous Orbit," ," AMOS Tech. Conf., Wailea, Hawaii, Sept, 2008.
4. Hujsak, R., "Solar Pressure," Proceedings of the Artificial Satellite Theory Workshop, USNO, Nov. 8-9, 1993, pp 54-72.
5. Vokrouhlicky, D., P. Farinella and F. Mignard, "Solar radiation pressure perturbations for Earth satellites: I. A complete theory including penumbra transitions," Astron. Astrophys. 280, 295-312, 1993.
6. Vokrouhlicky, D., P. Farinella and F. Mignard, "Solar radiation pressure perturbations for Earth satellites: II. An approximate method to model penumbra transitions and their long-term orbital effects on LAGEOS," Astron. Astrophys. 285, 333-343, 1994.
7. Marshall, J. Andrew and Scott B. Luthke, "Modeling Radiation Forces Acting on Topex/Poseidon for Precision Orbit Determination," Journal of Spacecraft and Rockets, Vol. 31, No. 1, January-February 1994.
8. Hujsak, Richard S., James W. Woodburn, John H. Seago, "The Orbit Determination Tool Kit (ODTK) – Version 5," AAS 07-125, AAS Astrodynamics Specialist Conference, Mackinac Island, MI, August 2007.
9. Wright, James, "Optimal Orbit Determination," Analytical Graphics, Inc., internal white paper, 2002.
10. Terejanu, G., Singla, P., Singh, T., Scott, P., (2008) "Uncertainty Propagation for Nonlinear Dynamical Systems using Gaussian Mixture Models," Journal of Guidance, Controls, and Dynamics Vol.31, No.6, pp. 1623-1633